Article

SOURCE DATA | TRANSPARENT PROCESS

EMBO reports

Infantile spasms-linked Nedd4-2 mediates hippocampal plasticity and learning via cofilin signaling

Kwan Young Lee[1], Jiuhe Zhu[1], Cathryn A Cutia[2], Catherine A Christian-Hinman[1,2,3], Justin S Rhodes[2,3,4] & Nien-Pei Tsai[1,2,3,*]

Abstract

Individuals affected by infantile spasms (IS), such as those carrying mutations in an IS-linked gene, neural precursor cell expressed developmentally downregulated gene 4-like (*Nedd4-2*), exhibit developmental delays and learning disabilities, but the underlying mechanism is unknown. Using conditional *Nedd4-2* knockout mice, we uncover that *Nedd4-2* functions to maintain the excitatory synapses in hippocampal neurons and allows for late-phase long-term synaptic potentiation (L-LTP) at Schaffer collateral synapses in the hippocampus. We also find that *Nedd4-2* is required for multiple forms of hippocampus-dependent learning and memory. Mechanistically, we show that loss of *Nedd4-2* leads to a decrease in actin polymerization caused by reduced phosphorylation of the actin depolymerizing protein cofilin. A cell-permeable peptide promoting phosphorylation of endogenous cofilin in *Nedd4-2* knockout neurons restores the number of hippocampal excitatory synapses and hippocampal L-LTP and partially restores hippocampus-dependent learning in mice. Taken together, our results reveal a novel mechanism underlying IS-associated learning disabilities and may provide information for future therapeutic strategies for IS.

Keywords cofilin; hippocampus-dependent learning; infantile spasm; Nedd4-2; synaptic plasticity

Subject Categories Cell Adhesion, Polarity & Cytoskeleton; Molecular Biology of Disease; Neuroscience

DOI 10.15252/embr.202152645 | Received 9 February 2021 | Revised 8 July 2021 | Accepted 15 July 2021

EMBO Reports (2021) e52645

Introduction

Infantile spasms (IS) represent a group of epileptic disorders occurring during infancy and early childhood. Although epileptic spasms usually resolve after 5 years of age, developmental delays and learning disabilities result in devastating consequences for many affected individuals and an ongoing major burden for their families and, ultimately, for the educational system in our society. In a recent retrospective study in which 133 individuals with IS were evaluated, 85% of them exhibited clinically documented developmental delays (Yuskaitis *et al*, 2018). Some cases of IS-associated developmental delay have been linked to seizure-induced structural changes in the brain, including changes in vasculature (Pavone *et al*, 2020), that subsequently lead to brain damage. However, developmental delays in many IS individuals without clear structural changes in the brain remain mysterious. Furthermore, because the developmental delays and learning disabilities in many IS individuals could be observed prior to the onset of spasms (Bednarek *et al*, 1998), it is speculated that the molecular mechanisms underlying learning disabilities in IS are different from those underlying epileptic spasms. Therefore, despite remarkable progress in recognizing infantile spasms over the years, the therapeutic intervention for IS-associated learning disabilities remains limited.

Similar to other types of epilepsies, many forms of IS are caused by *de novo* mutations in genes that are critically important in the brain. A previous study in which 264 childhood epilepsy patients were screened for *de novo* mutations identified neural precursor cell expressed developmentally downregulated gene 4-like (*Nedd4-2*) as one of the IS-associated genes (Allen *et al*, 2013). Reported from that study, one patient carrying a missense mutation in *Nedd4-2* developed IS and developmental delays that required special educational assistance later in school (Allen *et al*, 2013). A separate study reported that another patient carrying a different missense mutation in *Nedd4-2* also developed IS and neurodevelopmental deficits (Broix *et al*, 2016; Kato *et al*, 2017). These studies have prompted us to understand the role and function of *Nedd4-2* in the brain.

Nedd4-2 encodes a ubiquitin E3 ligase that is highly expressed in the brain. Nedd4-2 contains a C2 lipid-binding domain that guides Nedd4-2 to the cell membrane (Zhu *et al*, 2019). We and others have shown that Nedd4-2 ubiquitinates ion channels on the neuronal cell membrane to fine-tune neuronal excitability (Ekberg

1 Department of Molecular and Integrative Physiology, School of Molecular and Cellular Biology, University of Illinois at Urbana-Champaign, Urbana, IL, USA
2 Neuroscience Program, University of Illinois at Urbana-Champaign, Urbana, IL, USA
3 Beckman Institute for Advanced Science and Technology, University of Illinois at Urbana-Champaign, Urbana, IL, USA
4 Department of Psychology, University of Illinois at Urbana-Champaign, Champaign, IL, USA
*Corresponding author. Tel: +1 217 244 5620; Fax: +1 217 333 1133; E-mail: nptsai@illinois.edu

et al, 2007; Schuetz *et al*, 2008; Goel *et al*, 2015; Zhu *et al*, 2017; Kim *et al*, 2019). These findings support an earlier study that recognized *Nedd4-2* as an epilepsy-associated gene when mutations were identified in families with photosensitive generalized epilepsy (Dibbens *et al*, 2007). Although these past studies explain the contribution of impaired *Nedd4-2* to brain hyperexcitability in epilepsy, and likely also IS, we do not know how *Nedd4-2* may promote or ensure proper neurodevelopment and why impaired *Nedd4-2* leads to learning disabilities. Because the first documented IS patient carrying a missense mutation of *Nedd4-2* did not exhibit structural changes in the brain (Allen *et al*, 2013), it suggests that the developmental delays and learning disabilities may result from changes at the cellular level.

To test this possibility, we obtained a conditional *Nedd4-2* knockout (Nedd4-2 cKO) mouse model in which *Nedd4-2* is selectively reduced in the forebrain excitatory neurons. Our results showed that a loss of *Nedd4-2* in Nedd4-2 cKO mice leads to a reduced number of excitatory synapses in hippocampal neurons *in vitro* and to impaired late-phase long-term synaptic potentiation (L-LTP) at Schaffer collateral synapses in hippocampus *ex vivo*. Furthermore, the Nedd4-2 cKO exhibited defects in multiple forms of hippocampus-dependent learning and memory *in vivo*. Mechanistically, we found that the loss of *Nedd4-2* leads to reduced actin polymerization caused by cofilin dephosphorylation. Using a cell-permeable, phosphorylated, cofilin peptide that decoys dephosphorylation signaling and promotes phosphorylation of endogenous cofilin, we were able to restore the number of hippocampal excitatory synapses and hippocampal L-LTP and to partially restore hippocampus-dependent learning in Nedd4-2 cKO mice. Our findings suggest that *Nedd4-2* contributes to neurodevelopment and hippocampus-dependent learning through a mechanism different from those that *Nedd4-2* exerts to regulate neuronal excitability. Overall, our study reveals how *Nedd4-2* modulates hippocampal synaptic plasticity and provides critical information toward the development of therapeutic strategies for learning-disabled IS individuals especially for those who carry *Nedd4-2* mutations.

Results

Ablation of *Nedd4-2* impairs the functions of excitatory synapses and long-term synaptic plasticity in hippocampus

To study *Nedd4-2* in the brain, we first obtained a *Nedd4-2* floxed mouse model (*Nedd4-2*$^{f/f}$) in which exon 15 of the *Nedd4-2* allele is flanked with *loxP* sites (obtained from Dr. Hiroshi Kawabe at Max Planck Institute, Germany). Because we previously found that *Nedd4-2* is highly expressed in the excitatory neurons (Zhu *et al*, 2019), we then start by inhibiting *Nedd4-2* in the excitatory neurons. To this end, *Nedd4-2*$^{f/f}$ mice were crossed with *Emx1*-Cre mice to obtain *Nedd4-2*$^{f/f\text{-}Emx1\text{-}Cre+}$ (Nedd4-2 cKO) or *Nedd4-2*$^{f/f\text{-}Emx1\text{-}Cre-}$ (Nedd4-2 WT) mice (Fig 1A). *Emx1*-Cre can confer *Nedd4-2* deletion in forebrain excitatory neurons beginning as early as embryonic day 10.5 (Gorski *et al*, 2002), and we have confirmed an efficient reduction of Nedd4-2 in mouse forebrains (Fig 1A). Because *Nedd4-2* null mice are perinatal lethal (Boase *et al*, 2011), using *Nedd4-2* cKO mice permits viability and minimizes the concerns over specificity when using shRNA. To begin determining whether and how an impairment of *Nedd4-2* leads to learning disabilities, we assessed the synaptic transmission of hippocampal neurons by measuring the miniature excitatory postsynaptic currents (mEPSCs) in primary cultures made from Nedd4-2 WT or Nedd4-2 cKO mice at days *in vitro* (DIV) 14-17. As shown (Fig 1B), Nedd4-2 cKO neurons displayed a decrease in mEPSC frequency compared to Nedd4-2 WT neurons, whereas mEPSC amplitude did not differ between the two groups. mEPSC frequency can be correlated with the synapse number, whereas mEPSC amplitude is correlated with the strength of individual synapses (Pfeiffer & Huber, 2007; Niere *et al*, 2012). To test how *Nedd4-2* may regulate the number of synapses, we performed immunocytochemistry to quantify synapse numbers in primary hippocampal neuron cultures. On DIV 16, neurons were fixed and stained for the presynaptic marker Synapsin-I and the postsynaptic marker postsynaptic density protein 95 (PSD-95) to measure colocalization of pre- and postsynaptic puncta. As shown (Fig 1C), the synaptic puncta number, but not the averaged puncta area, was significantly reduced in Nedd4-2 cKO neurons when compared to Nedd4-2 WT neurons. Together, these data suggest that *Nedd4-2* is required for the maintenance or facilitation of excitatory synapses in hippocampal neurons.

To investigate the roles of *Nedd4-2* in hippocampal synaptic plasticity, we examined field excitatory postsynaptic potentials (fEPSPs) at Schaffer collateral synapses in hippocampus using acute hippocampal slices obtained from Nedd4-2 WT or Nedd4-2 cKO mice at 6–8 weeks of age (Fig 1D–G). We found no significant difference in stimulus-response and paired-pulse facilitation between Nedd4-2 WT and Nedd4-2 cKO mice (Fig 1D and E), suggesting that the basal transmission is intact in Nedd4-2 cKO hippocampal slices. We then measured long-term synaptic plasticity, including an early-phase long-term potentiation (E-LTP) induced by a single train of high-frequency stimulation (HFS; 100 Hz for 1 s) and a late-phase LTP (L-LTP) induced by four trains of HFS at 5-min intervals. As shown in Fig 1F, E-LTP did not differ between Nedd4-2 WT and Nedd4-2 cKO slices. In contrast, L-LTP was significantly reduced in Nedd4-2 cKO slices compared to Nedd4-2 WT slices (Fig 1G). The baseline fEPSPs without LTP induction were stable for at least 210 min in both Nedd4-2 WT and Nedd4-2 cKO slices (Fig EV1A and B), indicating the reduced L-LTP in Nedd4-2 cKO is not due to health of the slices or stability of the recordings. In conclusion, our results suggest that *Nedd4-2* is required for L-LTP at hippocampal Schaffer collateral synapses.

Nedd4-2 cKO mice exhibit deficits in hippocampus-dependent learning and memory

Long-term potentiation is considered one of the major cellular mechanisms that underlie learning and memory (Sudhof & Malenka, 2008; Takeuchi *et al*, 2014; Nicoll, 2017). Because our data suggest *Nedd4-2* is required for hippocampal L-LTP (Fig 1), we hypothesized that *Nedd4-2* is crucial to hippocampus-dependent learning and memory. To test this hypothesis, we began by employing male Nedd4-2 WT or Nedd4-2 cKO mice at 6–8 weeks of age for a series of behavioral experiments. To first determine the associative learning and memory, we conducted the contextual fear conditioning test (Fig 2A). During the training day, mice were placed in a training context and received brief aversive stimuli (footshock, 2×, 0.5 mA, 2 s duration, 30 s interval; Clark *et al*, 2008; Ujjainwala *et al*, 2019).

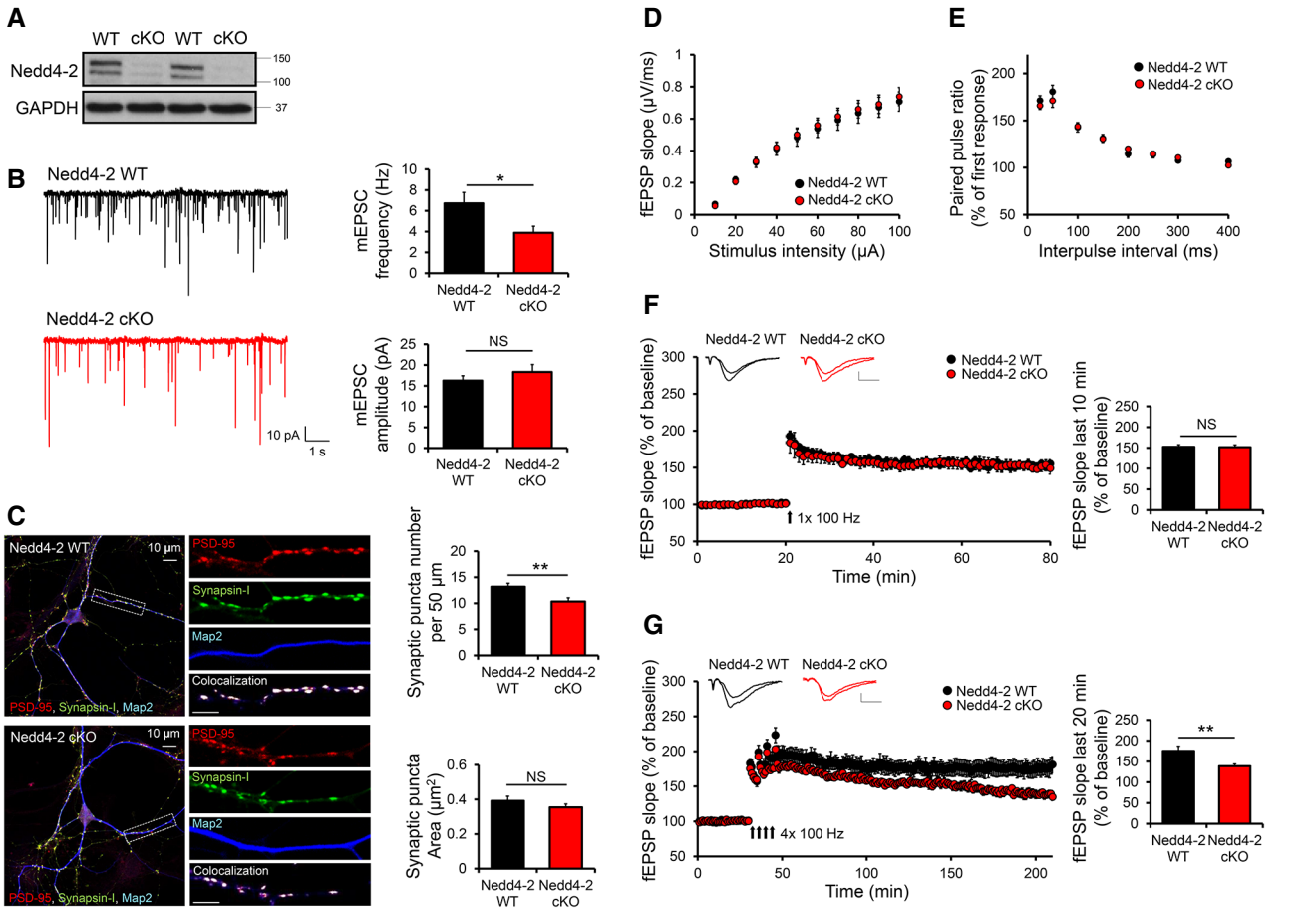

Figure 1. Nedd4-2 cKO mice exhibit alterations in hippocampal synaptic functions and L-LTP.

A Representative Western blots of Nedd4-2 and GAPDH from Nedd4-2 WT and Nedd4-2 cKO forebrains at postnatal day 14.

B Patch-clamp recording from Nedd4-2 WT or Nedd4-2 cKO cultured hippocampal neurons at DIV 14-17. Representative mEPSC traces (left) and quantification of mEPSC amplitude and frequency are shown (right) (n = 17 and 18 for Nedd4-2 WT and Nedd4-2 cKO neurons, respectively).

C Immunocytochemistry showing postsynaptic marker PSD-95 (red), presynaptic marker Synapsin-I (green), dendritic marker Map2 (blue), and colocalization of PSD-95 and Synapsin-I from dissociated Nedd4-2 WT or Nedd4-2 cKO hippocampal neurons at DIV 16. Representative secondary dendrites (left) and quantification of colocalized synaptic puncta number and area (right) (n = 36 for Nedd4-2 WT and Nedd4-2 cKO neurons) are shown. Scale bar: 5 μm.

D Synaptic input–output relationship was obtained by initial slope of fEPSPs against the stimulus intensity at Schaffer collateral synapses of hippocampal slices from Nedd4-2 WT (n = 14 slices from 11 mice) and Nedd4-2 cKO (n = 17 slices from 12 mice) mice at 6–8 weeks of age.

E Paired-pulse ratio of fEPSPs at Schaffer collateral synapses over an interpulse interval range of 25–400 ms from Nedd4-2 WT (n = 13 slices from 9 mice) and Nedd4-2 cKO (n = 12 slices from 8 mice) slices.

F A train of high-frequency stimulation (HFS; 100 Hz for 1 s) induced early-phase LTP (E-LTP) at Schaffer collateral synapses in Nedd4-2 WT (n = 7 slices from 6 mice) and Nedd4-2 cKO (n = 6 slices from 5 mice) mice. Representative fEPSP traces were recorded before and 60 min after LTP induction (Scale bars: 0.5 mV, 5 ms). Summary bar graphs showing the fEPSP slopes measured 50–60 min after a HFS at Schaffer collateral synapses were on the right.

G Late-phase LTP (L-LTP) induced by four trains of HFS in Nedd4-2 WT slices (n = 7 slices from 7 mice) and Nedd4-2 cKO slices (n = 9 slices from 8 mice). Representative fEPSP traces were recorded before and 180 min after LTP induction (Scale bars: 0.5 mV, 5 ms). Summary bar graphs showing the fEPSP slopes measured 160–180 min after L-LTP induction at Schaffer collateral synapses were on the right.

Data information: Student's t-test was used. Data are presented as mean ± SEM with $^*P < 0.05$, $^{**}P < 0.01$, and NS: non-significant.

On the test day (24 h after the training), mice were re-exposed to the training context and assessed for fear memory by measuring freezing behavior in the absence of footshock stimuli. As shown (Fig 2A), Nedd4-2 cKO mice exhibited a significant decrease in freezing behavior compared to Nedd4-2 WT mice. This effect is unlikely from an altered pain sensation because *Nedd4-2* exerts its function in pain specifically in dorsal root ganglion (DRG) neurons (Laedermann *et al*, 2013). In addition, Nedd4-2 WT and Nedd4-2 cKO mice exhibit similar postshock responses to the stimuli during the training day (Fig EV2A), confirming a similar sensitivity to the stimuli. Altogether, these data suggest that *Nedd4-2* is crucial to fear memory.

We then employed the Barnes maze to determine whether the loss of *Nedd4-2* impacts spatial reference memory (Fig 2B, left; Ujjainwala *et al*, 2019). The mice were first trained to escape a brightly lighted circular field by finding a dark escape hole. As shown (Fig 2B, top right), we found that Nedd4-2 cKO mice exhibited a significant increase in escape latency on the third and fourth

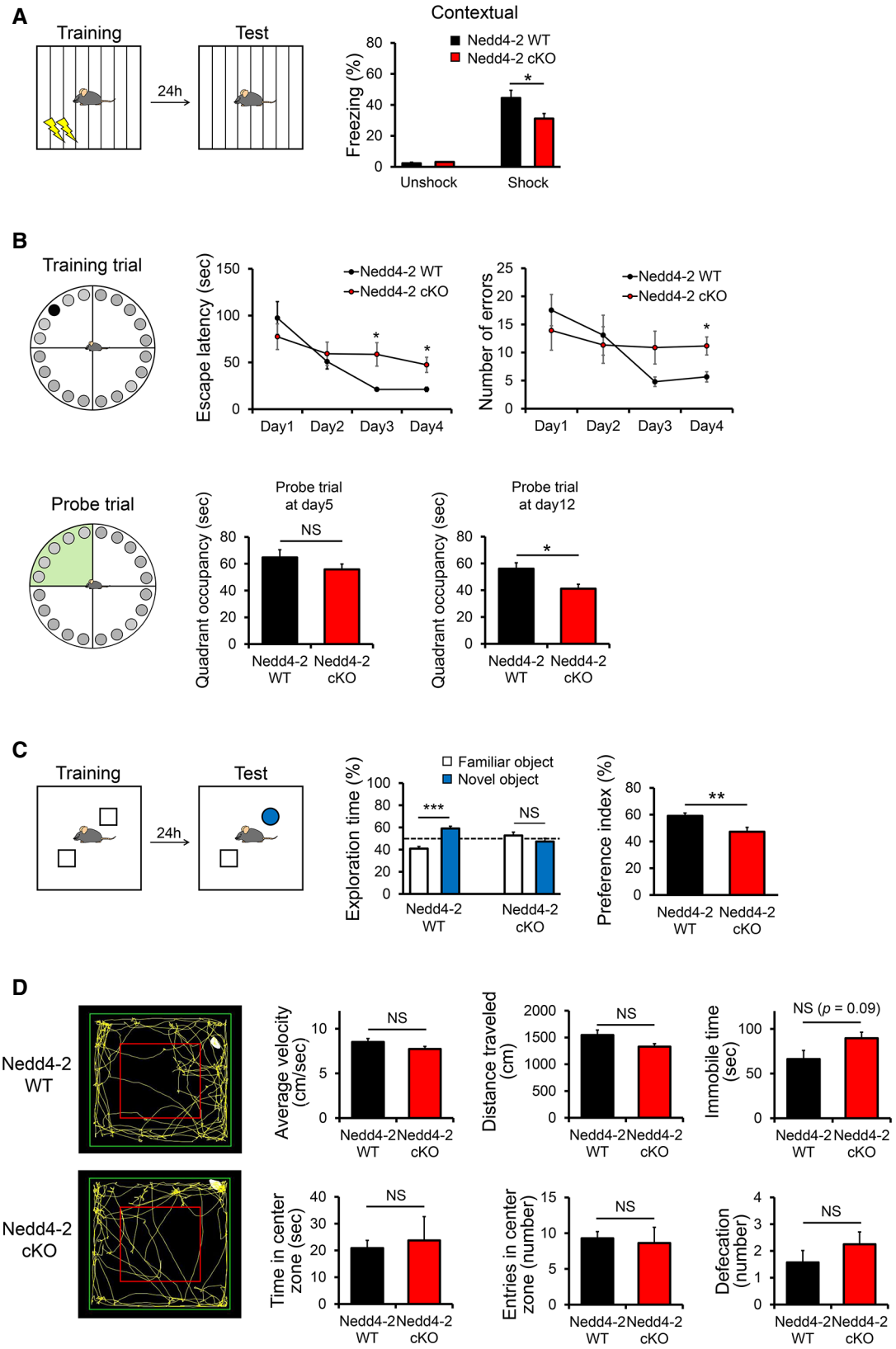

Figure 2.

Figure 2. Male Nedd4-2 cKO mice exhibit deficits in hippocampus-dependent learning and memory.

A Fear conditioning test from Nedd4-2 WT (n = 8) or Nedd4-2 cKO (n = 8) mice (6–8 weeks old). Schematic representation of fear conditioning test (left). Mice were placed in the fear conditioning chamber for 180 s with a metal grid floor and received two electrical shocks at 120 and 150 s (0.5 mV, 2 s). Twenty-four hrs later, mice were placed in the same chamber for 180 s in the absence of the shock. Freezing behavior during contextual fear conditioning test at 24 h after training is shown (right). Freezing rate from Nedd4-2 WT (n = 3) and Nedd4-2 cKO (n = 3) mice without shocks during the training (unshock) was also shown (right).

B Barnes maze test from Nedd4-2 WT (n = 8) or Nedd4-2 cKO (n = 8) mice (6–8 weeks old). Schematic representation of Barnes maze (top left). Mice were trained for 4 days with three training trials on each day to locate the escape box (black circle). Learning curve during 4 training days was shown by the escape latency and the number of errors before escaping (top right). Schematic representation of Barnes maze on probe trials (bottom left). Quadrant occupancy on probe trial at day 5 and at day 12 (bottom right) was assessed by the time spent in the target area (green quadrant).

C Novel object recognition test from Nedd4-2 WT (n = 8) or Nedd4-2 cKO (n = 8) mice (6–8 weeks old). Schematic representation of the test (left). Mice explored the chamber with two identical objects for 10 min during the training day. Twenty-four hrs later, mice returned to the chamber with one of the objects replaced by a novel object. Exploration time of familiar and novel objects on testing session (middle) and the preference index for the novel object (right) were measured. The dash line represents the 50% chance of exploring either of the objects.

D Open field test from Nedd4-2 WT (n = 7) and Nedd4-2 cKO (n = 8) mice. Representative image showing the explorative behavior of Nedd4-2 WT and Nedd4-2 cKO mice during 5-min open field test period (left). Quantification of locomotor activity and anxiety-like behavior is shown by average velocity, total distance traveled, immobile time, time spend in center zone, number of entries in center zone, and defecation number (right).

Data information: Student's t-test was used. Data are presented as mean ± SEM with $^{*}P < 0.05$, $^{**}P < 0.01$, $^{***}P < 0.001$, and NS: non-significant.

day of the training trial and an increase in number of exploring errors on the fourth day of the training trial, when compared to Nedd4-2 WT mice. To assess spatial memory formation, we then performed probe trials at days 5 and 12 in which the escape box under the target hole was removed (Fig 2B, bottom right). In the probe trial at day 5, Nedd4-2 WT and Nedd4-2 cKO mice exhibited similar quadrant occupancy. However, in the probe trial at day 12, Nedd4-2 cKO mice spent significantly less time in the target quadrant when compared to Nedd4-2 WT mice. These data suggest that *Nedd4-2* is crucial to spatial reference memory.

We next examined the mice in a novel object recognition test for recognition memory (Fig 2C; Lueptow, 2017; Ujjainwala *et al*, 2019). During the test, mice were placed in a testing box containing two identical objects and allowed to explore those objects for 10 min. Twenty-four hrs later, mice were returned to the box with one of the objects replaced by a new and unfamiliar object. The times during which the mice explored old versus new objects were then calculated. As shown (Fig 2C, middle), we found that Nedd4-2 WT mice, but not Nedd4-2 cKO mice, exhibited significant preference toward the novel object on the test day. This difference was also evident when comparing the preference index of Nedd4-2 WT and Nedd4-2 cKO mice (Fig 2C, right). On the contrary, when presenting both objects as novel to a new cohort of mice at the same time, both Nedd4-2 WT and Nedd4-2 cKO mice showed similar exploration time toward the two objects (Fig EV2B), suggesting the mice exhibit no preference or aversion to either of the objects. Altogether, these data indicate that *Nedd4-2* is crucial to recognition memory.

To rule out the possibility that the impaired learning behavior of Nedd4-2 cKO mice in the Barnes maze or novel object recognition test was a result of reduced overall exploring activity, we performed the open field test. As shown (Fig 2D), Nedd4-2 WT and Nedd4-2 cKO mice displayed similar levels of average speed, travel distance, immobile time, time spent in center zone, number of entries in center zone, and defecation. These data indicate similar exploring activity between Nedd4-2 WT and Nedd4-2 cKO mice.

To determine whether the behavioral outcomes that we observed are specific to male mice, we also conducted all four assays above using female mice. Surprisingly, except for a minor effect observed in Barnes maze test, female Nedd4-2 cKO mice showed comparable learning and memory behavior with female Nedd4-2 WT mice (Fig EV3A–C). Interestingly, the open field test revealed a reduced exploring activity in female Nedd4-2 cKO mice (Fig EV3D), which was not seen in male mice (Fig 2D). Altogether, our findings indicate sex-specific effects of *Nedd4-2* in behavior and suggest that *Nedd4-2* plays a critical role in hippocampus-dependent learning and memory particularly in male mice.

Actin dynamics are altered in *Nedd4-2* cKO mice

The actin cytoskeleton is crucial to many aspects of neurodevelopment including the formation and stability of excitatory synapses (Luo, 2002; Dillon & Goda, 2005; Cingolani & Goda, 2008). A previous study has suggested the role of Nedd4 family E3 ligases in axon growth (Hsia *et al*, 2014), indicating a possibility that Nedd4-2 may play a role in mediating actin dynamics. To test this possibility, we examined the filamentous (F)-actin to globular (G)-actin ratio, which reflects the balance between actin polymerization and depolymerization, in Nedd4-2 WT and Nedd4-2 cKO forebrains. As shown (Fig 3A), we found that the F-actin to G-actin ratio was reduced in Nedd4-2 cKO brains compared to that in Nedd4-2 WT brains, indicating a basally reduced actin polymerization in Nedd4-2 cKO mice. It has been established that long-term potentiation (LTP) is associated with an increase in F-actin to G-actin ratio (Fukazawa *et al*, 2003). We therefore asked whether *Nedd4-2* is also required for LTP-associated actin polymerization. To this end, we employed a chemically induced LTP (cLTP) protocol in cultured neurons at DIV 16, in which 200 μM glycine was applied to the cultures for 10 min to activate NMDA receptors (Fig 3B; Lu *et al*, 2001; Hussain *et al*, 2014). As shown, Nedd4-2 WT cultures exhibited an increase in F-actin to G-actin ratio after 10- or 30-min cLTP induction (Fig 3B, top right). However, cLTP induction in Nedd4-2 cKO neurons did not elevate F-actin to G-actin ratio (Fig 3B, bottom right), suggesting that *Nedd4-2* is required for LTP-induced actin polymerization.

Cofilin phosphorylation at serine-3 is impaired in *Nedd4-2* cKO mice

The actin dynamics can be regulated by an actin depolymerizing protein cofilin (Bamburg, 1999; Ohashi, 2015). Cofilin binds to both G-actin and F-actin which leads to actin depolymerization and

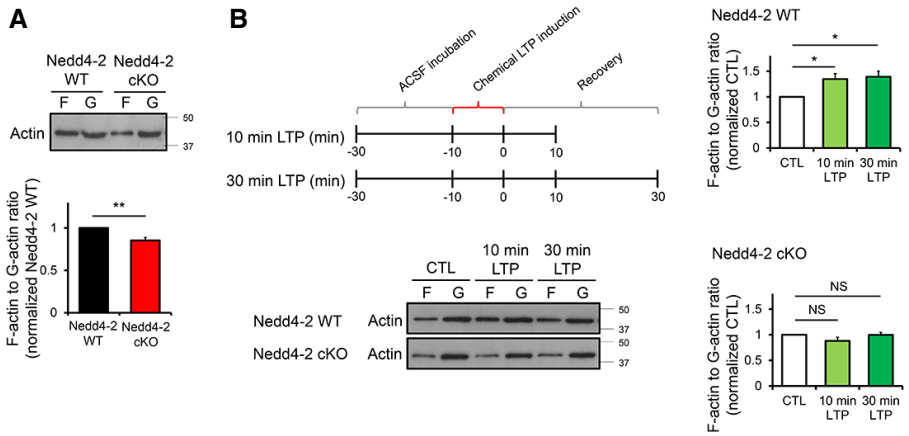

Figure 3. The actin dynamics is impaired in Nedd4-2 cKO mice during the basal state and upon induction of cLTP.

A Western blots of F-actin to G-actin ratio from Nedd4-2 WT or Nedd4-2 cKO forebrains at postnatal day 14. Representative Western blots and quantification are shown (n = 10 mice for Nedd4-2 WT and Nedd4-2 cKO).

B Western blots of F-actin to G-actin ratio with or without cLTP induction from Nedd4-2 WT or Nedd4-2 cKO cultured neurons. Schematic representation of the experimental design for cLTP inductions (top left). Representative Western blots (bottom left) and quantification of F-actin to G-actin from Nedd4-2 WT or Nedd4-2 cKO (right) cultures after cLTP induction and recovery in normal aCSF for 10 or 30 min before lysis (n = 11 and 8 for Nedd4-2 WT and Nedd4-2 cKO cultures, respectively). For quantification, data from cLTP induction were normalized to data from control (CTL) condition.

Data information: Student's t-test (A) and one-way ANOVA with Tukey test (B) were used. Data are presented as mean ± SEM with $^*P < 0.05$, $^{**}P < 0.01$, and NS: non-significant.
Source data are available online for this figure.

prevents reassembly of F-actin (Bamburg & Bernstein, 2010). Phosphorylation of cofilin at the serine-3 (S3) residue inhibits its binding to actin, which in turn promotes the elongation or stabilization of actin filaments (Moriyama *et al*, 1996; Ohashi, 2015). To test whether *Nedd4-2* modulates cofilin phosphorylation, we performed Western blot to detect cofilin and phospho (p)-cofilin on S3 residue and found that the levels of p-cofilin, but not total cofilin, were significantly reduced in Nedd4-2 cKO brains compared to Nedd4-2 WT brains (Fig 4A). To confirm our Western blot results in neuronal dendrites where LTP-associated actin polymerization occurs (Lin *et al*, 2005), we performed immunocytochemistry experiments using primary hippocampal neuron cultures to assess cofilin phosphorylation in dendrites. Consistent with our Western blot data, the levels of p-cofilin, but not total cofilin, were reduced in Nedd4-2 cKO dendrites compared to Nedd4-2 WT dendrites (Fig 4B). The reduced cofilin phosphorylation is likely resulted directly from the loss of *Nedd4-2* rather than a developmental defect because transiently expressing a *Nedd4-2* cDNA construct back to Nedd4-2 cKO neurons was able to restore cofilin phosphorylation to a level similar to that in Nedd4-2 WT neurons (Fig EV4A). Furthermore, because expressing an E3 ligase dead Nedd4-2 (C962A) failed to elevate cofilin phosphorylation, we conclude that the E3 ligase activity of Nedd4-2 is required for cofilin phosphorylation. Because cofilin phosphorylation is critical to F-actin formation during LTP (Fukazawa *et al*, 2003) and to hippocampus-associated learning (Rust *et al*, 2010), we next asked whether induction of LTP leads to *Nedd4-2*-dependent cofilin phosphorylation. As shown (Fig 4C), the levels of p-cofilin increased 10 or 30 min after induction of cLTP in Nedd4-2 WT neurons but not in Nedd4-2 cKO neurons. These data indicate that *Nedd4-2* is required for cofilin phosphorylation during the basal state and upon induction of LTP.

Inhibition of cofilin restores synaptic deficits in Nedd4-2 cKO neurons

To determine whether the synaptic deficits that we observed in Nedd4-2 cKO mice (Fig 1) are due to reduced cofilin phosphorylation, we asked whether inhibition of cofilin through promoting cofilin phosphorylation could restore synaptic function in Nedd4-2 cKO hippocampal neurons. To this end, we used a cell-permeable TAT-phospho-cofilin (TAT-pS3) peptide that has been extensively used previously to decoy dephosphorylation signaling and promote phosphorylation of endogenous cofilin (Yuen & Yan, 2009; Duffney *et al*, 2013; Wang *et al*, 2013). Following the incubations of control TAT, non-phosphorylated TAT-S3 or the phosphorylated TAT-pS3 peptides (10 μM) for 12–16 h, as previously described (Duffney *et al*, 2013), in Nedd4-2 WT or Nedd4-2 cKO hippocampal neuron cultures on DIV 14-17, we measured the number of synaptic puncta and mEPSCs as we performed in Fig 1. As shown (Fig 5A and B), treatment of TAT-S3 peptide reduced the synaptic puncta number and mEPSC frequency in Nedd4-2 WT neurons since non-phosphorylated TAT-S3 is known to reduce phosphorylation of endogenous cofilin and actin polymerization as reported previously (Li *et al*, 2014). However, most importantly, the phosphorylated TAT-pS3 peptide was able to increase the synaptic puncta number and mEPSC frequency in Nedd4-2 cKO neurons, without significant changes in synaptic puncta area or mEPSC amplitude (Fig 5 A and B). Because cofilin is highly phosphorylated in Nedd4-2 WT neurons (Fig 4), as expected, TAT-pS3 peptide did not exert significant effects on Nedd4-2 WT neurons.

To determine whether inhibition of cofilin can also restore the impaired L-LTP that we observed in Nedd4-2 cKO hippocampal slices (Fig 1G), we preincubated Nedd4-2 WT and Nedd4-2 cKO hippocampal

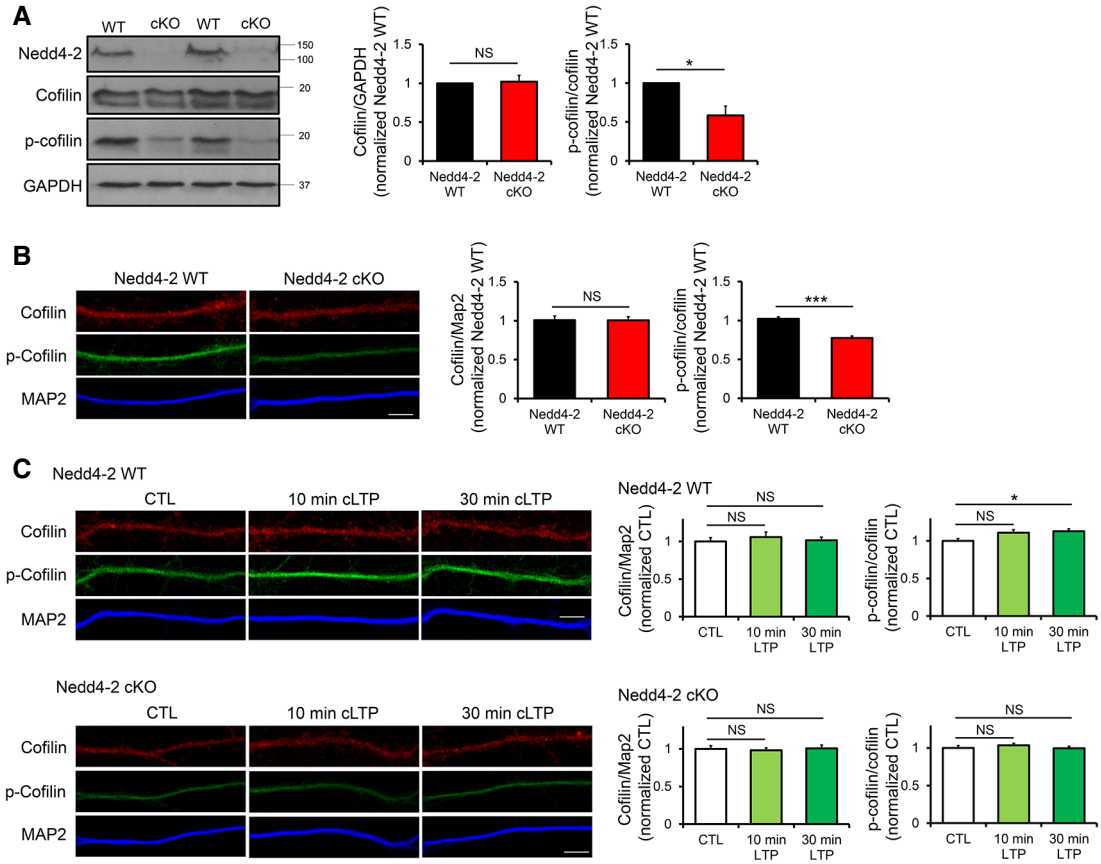

Figure 4. Cofilin phosphorylation is impaired in Nedd4-2 cKO mice.

A Western blots of Nedd4-2, total cofilin, phospho (p)-cofilin, and GAPDH from Nedd4-2 WT or Nedd4-2 cKO forebrains at postnatal day 14. Representative Western blots and quantification of total cofilin relative to GAPDH and p-cofilin relative to total cofilin (n = 6 for Nedd4-2 WT and Nedd4-2 cKO brains) were shown.

B Immunocytochemistry of cofilin, p-cofilin, and dendritic marker MAP2 from Nedd4-2 WT or Nedd4-2 cKO cultured hippocampal neurons at DIV 16. Representative dendrites of Nedd4-2 WT and Nedd4-2 cKO neurons and quantification of total cofilin relative to MAP2 and p-cofilin relative to total cofilin are shown (n = 25 and 26 for Nedd4-2 WT and Nedd4-2 cKO neurons, respectively). Scale bar: 5 μm.

C Immunocytochemistry showing cofilin, p-cofilin, and dendritic marker MAP2 from Nedd4-2 WT or Nedd4-2 cKO cultured hippocampal neurons induced with or without cLTP at DIV 16. Representative dendrites and quantification from Nedd4-2 WT or Nedd4-2 cKO cultures are shown (n = 36–39 neurons). Scale bar: 5 μm. For quantification, data from cLTP induction were normalized to data from control (CTL) condition.

Data information: Student's t-test (A, B) and one-way ANOVA with Tukey test (C) were used. Data are presented as mean ± SEM with $^*P < 0.05$, $^{***}P < 0.001$, and NS: non-significant.

slices with TAT or TAT-pS3 (20 μM) peptides for 1 h before the fEPSP recordings. While the TAT-pS3 peptide did not affect L-LTP in Nedd4-2 WT slices (Fig 5C, left), TAT-pS3 peptide was able to significantly improve L-LTP in Nedd4-2 cKO slices (Fig 5C, right). Together, these data indicate that TAT-pS3 treatment could rescue the synaptic puncta number and mEPSC frequency in Nedd4-2 cKO hippocampal neurons and L-LTP in Nedd4-2 cKO hippocampal slices.

Inhibition of cofilin partially restores hippocampus-dependent learning and memory in Nedd4-2 cKO mice

Because inhibition of cofilin was able to restore excitatory synapses and synaptic function in Nedd4-2 cKO neurons (Fig 5), we aimed to determine whether inhibition of cofilin could improve learning and memory behavior in Nedd4-2 cKO mice. To this end, Nedd4-2 WT or Nedd4-2 cKO mice were given an intraperitoneal injection of TAT (2 mg/kg) or TAT-pS3 (2 mg/kg) peptide 24 h before each behavioral task (Fig 6A). The route of injections and the dosage were chosen based on a previously published protocol (Wu *et al*, 2015), and we have observed an effective elevation of cofilin phosphorylation in the brain of Nedd4-2 cKO mice following the injections (Fig EV4B). We then employed the fear conditioning test to assess the fear memory. As shown (Fig 6B), TAT-pS3 peptide did not change freezing behavior in Nedd4-2 WT mice, but significantly improved the freezing behavior in Nedd4-2 cKO mice. We then employed the Barnes maze test to assess the spatial reference memory (Fig 6C). In Nedd4-2 WT mice, no significant difference was observed in the performance from mice receiving either TAT or TAT-pS3 peptides (Fig 6C, top). Interestingly, although TAT-pS3 peptide did not produce significant effects in Nedd4-2 cKO mice on training trials or probe trial at day 5, it significantly improved the quadrant occupancy of Nedd4-2 cKO mice on probe trial at day 12

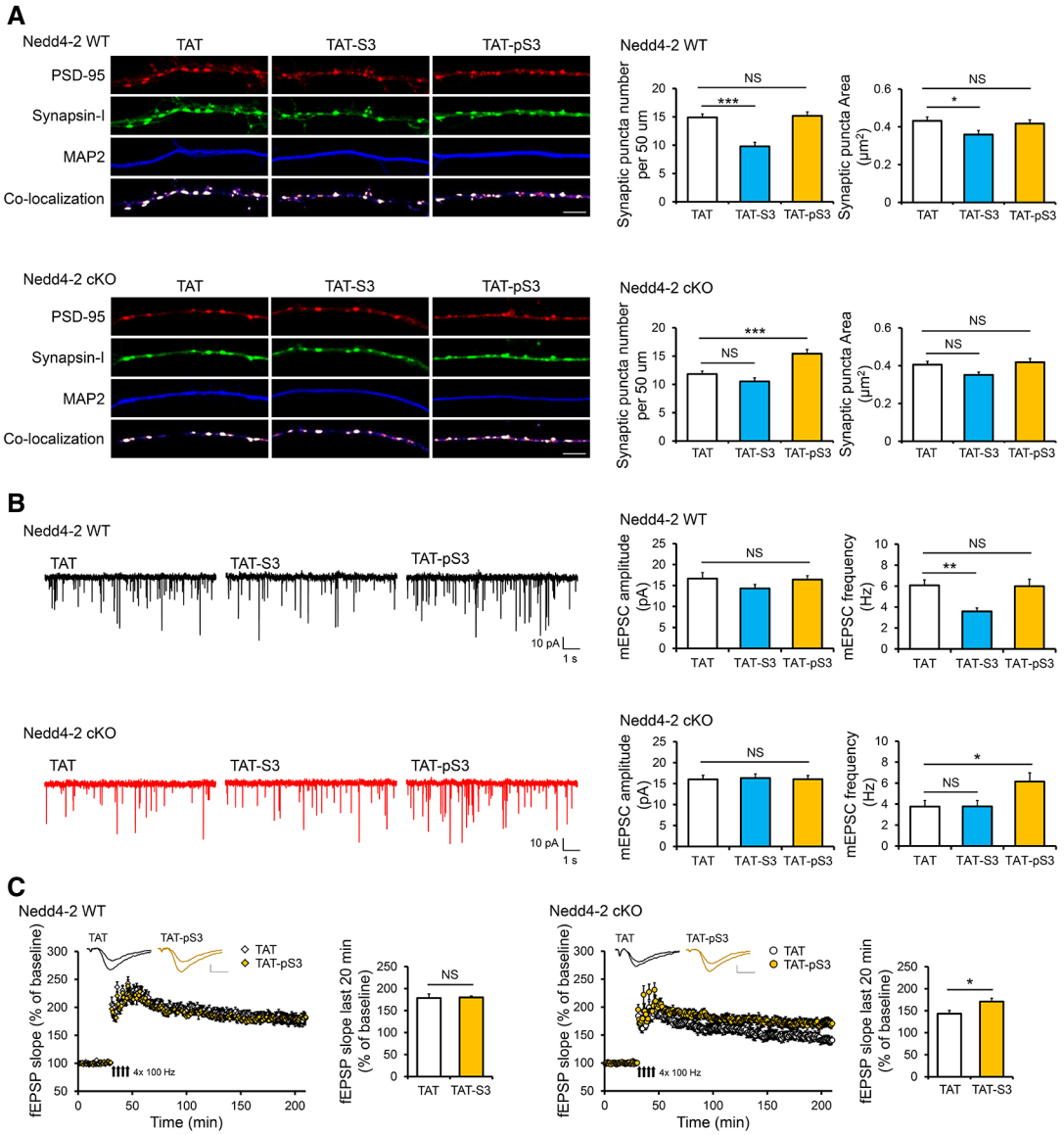

Figure 5. Inhibition of cofilin restores hippocampal synaptic functions and L-LTP in Nedd4-2 cKO mice.

A Immunocytochemistry showing postsynaptic marker PSD-95 (red), presynaptic marker Synapsin-I (green), dendritic marker Map2 (blue), and colocalization of PSD-95 and Synapsin-I from Nedd4-2 WT or Nedd4-2 cKO cultured hippocampal neurons at DIV 16 treated with TAT, TAT-S3, or TAT-pS3 peptide for 12 h (10 μM). Representative secondary dendrites of Nedd4-2 WT (top left) and Nedd4-2 cKO (bottom left) neurons are shown. Quantification of colocalized synaptic puncta number and synaptic puncta area for Nedd4-2 WT (top right) and Nedd4-2 cKO (bottom right) neurons is on the right (n = 32–36 neurons). Scale bar: 5 μm.

B Patch-clamp recordings from Nedd4-2 WT or Nedd4-2 cKO hippocampal neurons treated with TAT, TAT-S3, or TAT-pS3 peptide for 12 h (10 μM) at DIV 14-17. Representative mEPSC traces from Nedd4-2 WT (top left) and Nedd4-2 cKO (bottom left) are shown. Quantification of mEPSC amplitude and frequency from Nedd4-2 WT (top right) and Nedd4-2 cKO (bottom right) neurons are shown (n = 22–24 neurons).

C fEPSP recording from Nedd4-2 WT (left; n = 7 slices from 6 mice for TAT and n = 6 slices from 6 mice for TAT-pS3) and Nedd4-2 cKO (right; n = 9 slices from 9 mice for both TAT and TAT-pS3) hippocampal slices of mice at age 6–8 weeks. The slices were pretreated with TAT or TAT-pS3 peptide (20 μM) for 1 h before the induction of L-LTP at Schaffer collateral synapses. Representative fEPSP traces were recorded before and 180 min after LTP induction (scale bars: 0.5 mV, 5 ms). Summary bar graphs showed the fEPSP slopes measured 160–180 min after L-LTP induction at Schaffer collateral synapses.

Data information: One-way ANOVA with Tukey test (A, B) and Student's t-test (C) were used. Data are presented as mean ± SEM with *P < 0.05, **P < 0.01, ***P < 0.001, and NS: non-significant.

(Fig 6, bottom). Lastly, we employed the novel object recognition test to assess recognition memory. As shown (Fig 6D), the TAT-pS3 peptide did not improve the exploration time or preference index in Nedd4-2 cKO mice, suggesting a possibility that other downstream pathways of *Nedd4-2* are involved in this learning behavior. Taken together, our findings indicate that inhibition of cofilin by TAT-pS3 peptide partially restored hippocampus-dependent learning and memory behavior in Nedd4-2 cKO mice.

Because *Nedd4-2* encodes a E3 ubiquitin ligase and we have shown that its ligase activity is critical to cofilin phosphorylation (Fig EV4A), we suspect that Nedd4-2 modulates the levels of kinases or phosphatases for cofilin to regulate cofilin phosphorylation. To test this idea, we performed Western blot using Nedd4-2 WT and Nedd4-2 cKO forebrain lysates against multiple kinases and phosphatases known to mediate cofilin phosphorylation, including protein phosphatase 1 (PP1), protein phosphatase 2A (PP2A), Ca^{2+}/calmodulin-dependent protein kinase II α and β (CaMKIIα and CaMKIIβ), protein phosphatase Slingshot homolog 1 (SSH1) and phosphorylated SSH1 at serine-978, LIM domain kinase 1 (LIMK1) and phosphorylated LIMK1 at threonine 508, and phosphatase chronophin (Epstein *et al*, 1989; Ambach *et al*, 2000; Oleinik *et al*, 2010; Mizuno, 2013; Hu *et al*, 2014; Chen *et al*, 2018). However, as

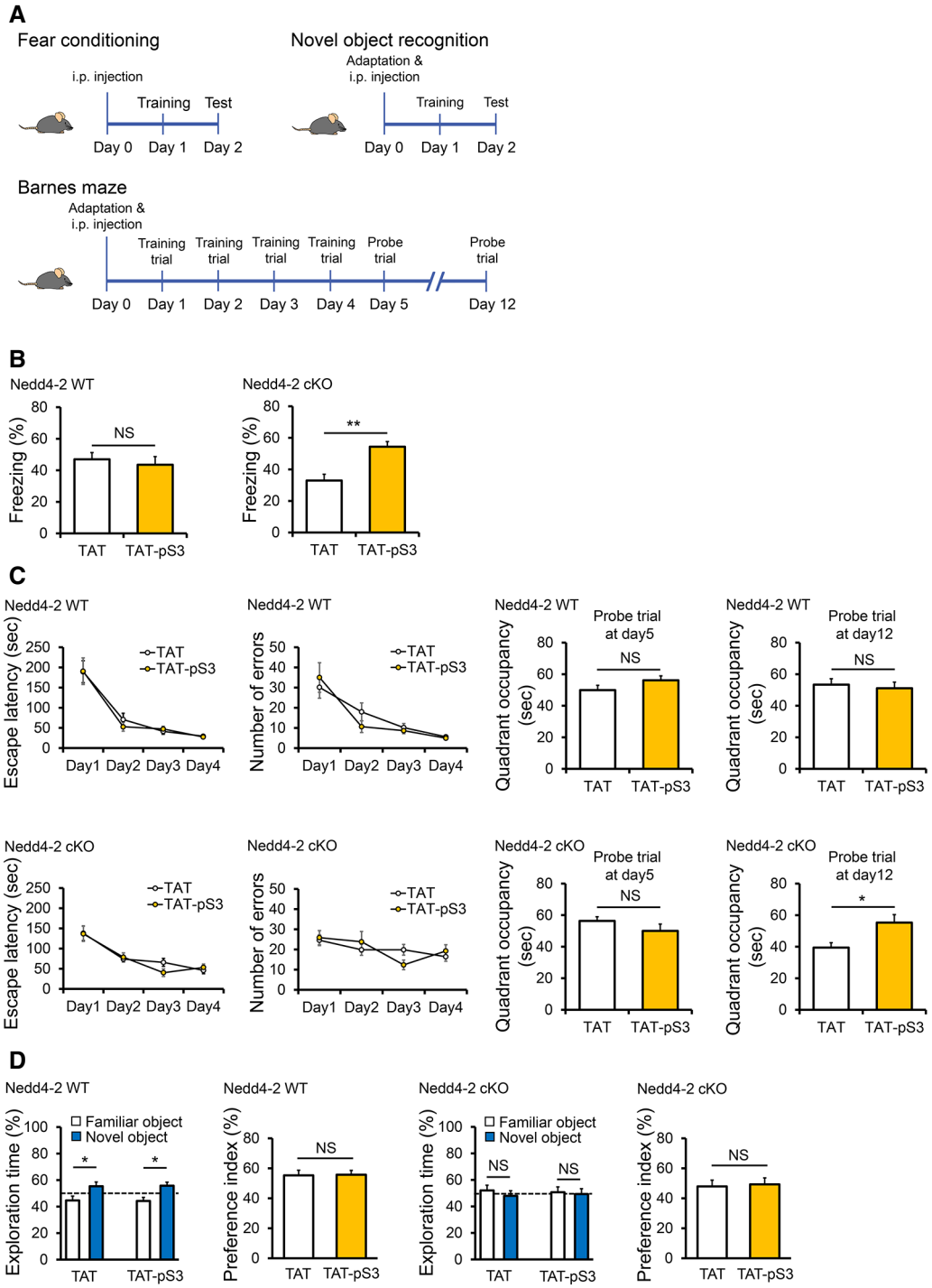

Figure 6.

Figure 6. Inhibition of cofilin partially restores learning and memory behavior in Nedd4-2 cKO mice.

A Experimental scheme for contextual fear conditioning, Barnes maze, and novel object recognition tests with intraperitoneal injections of TAT or TAT-pS3 peptide (2 mg/kg) in Nedd4-2 WT or Nedd4-2 cKO mice at 6–8 weeks of age.

B Quantification of freezing behavior in a fear conditioning test after intraperitoneally injecting TAT or TAT-pS3 peptides in Nedd4-2 WT mice (left) or Nedd4-2 cKO mice (right) ($n = 8$).

C Barnes maze test after intraperitoneally injecting TAT ($n = 8$) or TAT-pS3 ($n = 8$) peptide in Nedd4-2 WT mice (top), or TAT ($n = 9$) or TAT-pS3 ($n = 8$) peptides in Nedd4-2 cKO mice (bottom). Learning curve during 4 training days of Barnes maze task showing the escape latency and number of errors before escaping, and the quadrant occupancy on probe trial at day 5 and at day 12 was assessed.

D Novel object recognition test after intraperitoneally injecting TAT or TAT-pS3 peptides in Nedd4-2 WT mice (left) or Nedd4-2 cKO mice (right) ($n = 8$). Exploration time on familiar and novel objects and preference index for the novel object on testing session were shown. The dash line represents the 50% chance of exploring either of the objects.

Data information: Student's *t*-test was used. Data are represented as mean ± SEM with $*P < 0.05$, $**P < 0.01$, and NS: non-significant.

shown in Fig EV5A–E, we did not detect significant differences between Nedd4-2 WT and Nedd4-2 cKO in any of these proteins, suggesting a possibility that an unknown kinase, phosphatase, or regulatory mechanism is involved in *Nedd4-2*-dependent cofilin phosphorylation.

Discussion

Our study provides a mechanistic understanding of how *Nedd4-2* is crucial to hippocampal synaptic plasticity and learning (Fig 7). Our results also suggest that insufficient or improper functions of *Nedd4-2* disrupt different downstream pathways contributing to brain hyperexcitability and to learning disabilities. Specifically, we and others have shown that impaired ubiquitination of multiple ion channels is responsible for neuronal hyperexcitability when *Nedd4-2* is reduced (Ekberg *et al*, 2007; Schuetz *et al*, 2008; Goel *et al*, 2015; Zhu *et al*, 2017), suggesting that inhibition of certain ion channels might be a suitable treatment plan for *Nedd4-2*-associated epilepsy or IS. In this current study, we showed that abnormally dephosphorylated cofilin contributes to impaired hippocampal synaptic plasticity and to learning disabilities in the absence of *Nedd4-2*, indicating that an increase of cofilin phosphorylation or an inhibition of cofilin–actin interaction could potentially be useful for addressing those defects. However, it remains unclear how *Nedd4-2* modulates cofilin phosphorylation. We have tested several known kinases and phosphatases for cofilin but did not find significant changes in their expression when *Nedd4-2* is reduced. There is a possibility that Nedd4-2 modulates the expression of an unknown kinase or phosphatase for cofilin. Another possibility is that Nedd4-2 modulates cofilin phosphorylation through indirect signaling pathways associated with cofilin. For example, integrin signaling is known to indirectly regulate cofilin phosphorylation through Rho GTPases (Toshima *et al*, 2001). Because integrin signaling is initiated on the cell membrane where a portion of Nedd4-2 is localized (Zhu *et al*, 2019), there is a possibility that Nedd4-2 interconnects integrins or other membrane protein signaling to affect cofilin. We aim to test this possibility in the future.

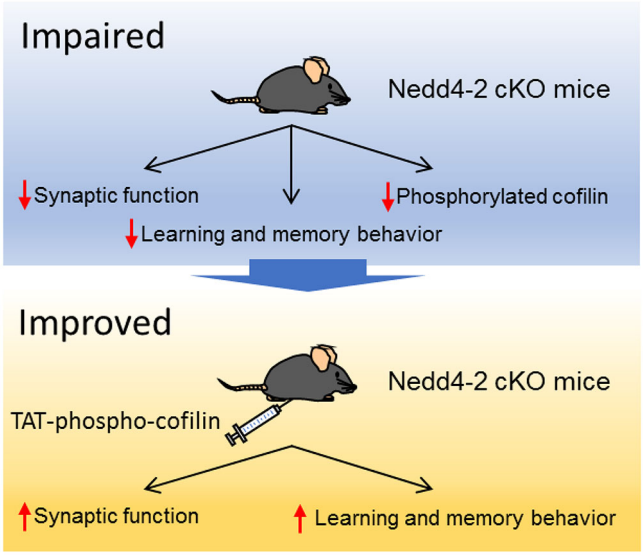

Figure 7. A diagram summarizing the defects in Nedd4-2 cKO mice and the improvement in mice following administration of phosphorylated TAT-cofilin peptide.

Given the complex functions of *Nedd4-2*, several other future research directions are being considered. First, while our current study demonstrated the defects when *Nedd4-2* is absent, whether similar effects can be observed when *Nedd4-2* contains missense mutations remains to be determined. Our previous work has shown that three epilepsy-associated mutations, located on or near the substrate recognition WW domains, exhibit reduced interaction toward selective substrates. The two reported mutations on *Nedd4-2* leading to IS and developmental delays, however, are both located on the homolog to the E6-AP carboxyl terminus (HECT) ligase domain (Broix *et al*, 2016; Kato *et al*, 2017). Presumably, such mutations on HECT domain could have more profound effects on E3 ligase activity of Nedd4-2 and may affect a broad spectrum of substrates in the brain. However, it remains to be determined whether those mutations lead to gain-of-function or loss-of-function effects on Nedd4-2 and to what extent those mutations alter cofilin phosphorylation.

Second, while our data showed a *Nedd4-2*-dependent elevation of cofilin phosphorylation following LTP induction, it would be interesting to know whether such an effect can also be seen by other neuronal stimulations. For example, the level of Nedd4-2 can be elevated following chronic activity stimulation during homeostatic downscaling (Jewett *et al*, 2015). Based on our study, it is expected that cofilin phosphorylation can likely be elevated by chronic activity stimulation. If so, it could suggest a role of cofilin phosphorylation in homeostatic plasticity.

Third, the relative contribution of two major *Nedd4-2* isoforms to neurodevelopment and learning remains unknown. The C2 domain-

lacking isoform of Nedd4-2 is primarily located in the cytoplasm and has a different pool of substrates, based on our recent study (Zhu *et al*, 2019). It would be important to know whether both of the *Nedd4-2* isoforms (C2-containing and C2-lacking isoforms) are responsible for modulating cofilin phosphorylation. Although all the currently known disease-associated mutations can be found in both isoforms, the pathophysiological outcomes resulting from different isoforms may be different due to different pools of substrates of the two isoforms. Therefore, further study on the differential effects of two major *Nedd4-2* isoforms on cofilin signaling will be needed to answer this question.

Lastly, in addition to the molecular pathways, another interesting finding from our study worth of exploring in the future is the sex-specific role of *Nedd4-2* in behavior. Specifically, we found that the loss of *Nedd4-2* impairs learning and memory in male mice but reduces overall exploring activity in female mice. These results suggest that Nedd4-2 may have different substrates and/or different activity toward certain substrates in males versus in females. This could add another layer of complexity about sex-specific behavior since cofilin signaling is known to be regulated sex-dependently (Baharani *et al*, 2020). Reduced exploring activity of female Nedd4-2 cKO mice in an open field test could suggest altered motor function and/or anxiety behavior, which have both been linked to IS (Price *et al*, 2009; Asinof *et al*, 2016; Salar *et al*, 2018). Because *Nedd4-2* is known to regulate locomotor activity (Yanpallewar *et al*, 2016; Kim *et al*, 2021), it would be important to know, as a future direction, whether actin polymerization is impaired in other parts of the brain, such as the cerebellum, when *Nedd4-2* is absent, and if yes, whether a sex-specific effect can be observed.

In conclusion, our study provides the first evidence to demonstrate how the IS-associated gene *Nedd4-2* mediates hippocampal learning and memory. Together with early detection and treatment for IS, we hope our results can lead to future development of early intervention for developmental delays and learning disabilities associated with *Nedd4-2*-dependent IS.

Materials and Methods

Ethics statement

All experiments using animals followed the guidelines of Animal Care and Use provided by the Illinois Institutional Animal Care and Use Committee (IACUC) and the guidelines of the Euthanasia of Animals provided by the American Veterinary Medical Association (AVMA) to minimize animal suffering and the number of animals used. This study was performed under an approved IACUC animal protocol of University of Illinois at Urbana-Champaign (#17075 and #20049 to N.-P. Tsai.).

Mice and genotyping

Nedd4-2 floxed mice in C57BL/6J background were obtained from Dr. Hiroshi Kawabe (Max Planck Institute, Göttingen, Germany), and *Emx1*-Cre mice also in C57BL/6J background were obtained from The Jackson Laboratory. Mice were group-housed in a 12-h light/dark cycle in a temperature-controlled room with *ad libitum* access to water and food. For genotyping, the primers used to detect *Nedd4-2 loxP* alleles are 5'-TCCCCACTGCAGTTCCTACC-3' and 5'-AGCTGCTCAGGCTGAATCACC-3'. PCR was performed using the program as below: 3 min at 94°C; 5 cycles of 20 s at 94°C, 20 s at 65°C, 2 min at 72°C; 5 cycles of 20 s at 94°C, 20 s at 60°C, 2 min at 72°C; 25 cycles of 20 s at 94°C, 20 s at 55°C, 2 min at 72°C; and 10 min at 72°C. The primers used to detect *Emx1*-Cre alleles are 5'-CGGTCTGGCAGTAAAAACTATC-3' (*Emx1-Cre*), 5'-GT GAAACAGC ATTGCTGTCACTT-3' (*Emx1-Cre*), 5'-AAGGTGTGGTTCCAGAATCG-3' (*Wild type*), and 5'-CTCTCCACCAGAAGGCTGAG- 3' (*Wild type*). PCR was performed using the program as below: 2 min at 94°C; 10 cycles of 20 s at 94°C, 15 s at 65°C (with 0.5°C per cycle decrease), 10 s at 68°C; 28 cycles of 15 s at 94°C 15 s at 60°C, 10 s at 72°C; and 2 min at 72°C.

Reagents and antibodies

Dimethyl sulfoxide (BP231) was from Thermo Fisher Scientific. Tetrodotoxin (TTX, 14964) was from Cayman Chemical. Picrotoxin (sc-202765) was from Santa Cruz Biotechnology. Bicuculline (2503) was from Tocris. Strychnine (S8753) was from Sigma. Glycine (CG01) was from Bioland Scientific. TAT peptide (TAT, RKKRRQRRR), TAT-cofilin peptide (TAT-S3, RKKRRQRRRMASGVAVSDGVIKVFN), and TAT-phospho-cofilin peptide (TAT-pS3, RKKRRQRRRMA(pSer) GVAVSDGVIKVFN) were synthesized by LifeTein. Mouse monoclonal anti-PSD-95 antibody (sc-32290) and mouse monoclonal anti-cofilin (sc-53934) antibody were from Santa Cruz Biotechnology. Rabbit polyclonal anti-Synapsin-I (ab8), chicken polyclonal anti-Microtubule-associated protein 2 (MAP2, ab92434), rabbit monoclonal anti-PP1 (ab52619), and rabbit polyclonal anti-phospho T508-LIMK1 (ab38508) were from Abcam. Rabbit polyclonal anti-Nedd4-2 (4013), rabbit monoclonal anti-phospho S3-Cofilin (3313), rabbit monoclonal anti-Cofilin (5175), rabbit polyclonal anti-CaMKII (3362), rabbit polyclonal anti-LIMK1 (3842), rabbit monoclonal anti-Chronophin (4686), and horseradish peroxidase (HRP)-conjugated anti-mouse secondary antibody (7076) were from Cell Signaling Technology. Rabbit polyclonal anti-PP2A alpha (PA5-17510), anti-mouse Alexa Fluor 488 (A-11001), anti-rabbit Alexa Fluor 555 (A-21428), and anti-chicken Alexa Fluor 633 (A-21103) were from Thermo Fisher Scientific. Mouse monoclonal anti-Actin (MAB1501) was from Sigma. Mouse monoclonal anti-GAPDH (60004-1-Ig) was from ProteinTech. Rabbit polyclonal anti-SSH1L (SP1711) and rabbit polyclonal anti-phospho S978-SSH1L (SP3901) were from ECM Biosciences. HRP-conjugated anti-rabbit secondary antibody (711-035-152) was from Jackson ImmunoResearch.

Primary neuronal cultures

Primary neuronal culture was performed as described previously (Zhu *et al*, 2019). Briefly, cortices or hippocampi were isolated from mixed-sex mice aged at postnatal day 0-1, digested with trypsin (T479; Sigma), and plated on poly-D-lysine (0.05 mg/ml; sc-136156; Santa Cruz Biotechnology)-coated glass coverslips for mEPSC recordings and immunocytochemistry or 10-cm plastic plate for Western blot. The cultures were maintained in NeuralA basal medium (10888022; Thermo Fisher Scientific) supplemented with B27 supplement (17504001; Invitrogen), GlutaMax (final concentration at 2 mM; 35050061; Invitrogen), and cytosine β-D-arabinofuranoside (AraC, final concentration at 1 μM; C1768;

Sigma). Each experiment was performed using sister cultures made from the same litter. Cultures were grown at 37°C with 5% carbon dioxide atmosphere. The culture medium was changed 50% on days *in vitro* (DIV) 2 and every 3–4 days thereafter until the experiments on DIV 14-17.

Immunocytochemistry and imaging

Immunocytochemistry was done as previously described (Lee *et al*, 2018). In brief, primary hippocampal neurons grown on poly-D-lysine-coated coverslips were fixed at DIV 16 with fixation buffer (4% paraformaldehyde and 4% sucrose in phosphate-buffered saline (PBS)) for 20 min and permeabilized with 0.2% Triton X-100 in PBS for 10 min. The coverslips were blocked in 1% bovine serum albumin (BSA, BP9706100; Thermo Fisher Scientific) in PBS for 30 min and incubated with primary antibodies for overnight at 4°C. After three 10-min washings with PBS, the coverslips were subsequently incubated with fluorescence-conjugated secondary antibodies for 2 h at room temperature (23–25°C). After final washes with PBS, coverslips were mounted onto glass slides. Images were obtained using a Zeiss LSM 700 confocal microscope with 40× magnification and three different lasers (488, 555, and 633 nm). Pinhole was set to 1 airy unit for all experiments. Confocal microscope settings were kept with the same scanning configurations to allow for comparison across conditions. For image analysis, the background-subtracted mean fluorescence intensity in 3 secondary dendritic regions of 50 μm was analyzed per cell using ImageJ software (National Institute of Health) (Tsai *et al*, 2012). The background signal was obtained from 3 nearby areas without any cells from the same image.

Western blot

For Western blot, forebrains or cultured neurons were isolated and homogenized in cold lysis buffer containing (in mM): 137 Nacl, 20 Tris–HCl, 2 EDTA, 1% Triton X-100 (pH 8.0) supplemented with protease inhibitor (A32963; Thermo Fisher Scientific) and phosphatase inhibitor (P2850; Sigma). Protein concentration was measured using the Bradford assay. Samples were resolved on SDS–PAGE and transferred onto a polyvinylidene fluoride (PVDF) membrane (sc-3723; Santa Cruz Biotechnology). After blocking with a 1% BSA solution in Tris-buffered saline with Tween-20 (TBST, 20 mM Tris pH 7.5, 150 mM NaCl, 0.1% Tween-20) for 30 min, the membrane was incubated with primary antibody overnight at 4°C, followed by three 10-min washings with the TBST. The membrane was then incubated with an HRP-conjugated secondary antibody in 5% non-fat milk in TBST for 1 h at room temperature (23–25°C), followed by another three 10-min washings. Finally, the membrane was developed with an ECL Chemiluminescent Reagent and X-ray films (Jewett *et al*, 2015; Liu *et al*, 2019). Signals from the proteins of interest were normalized to the house-keeping protein GAPDH. For the phospho-specific proteins, the phospho-specific signals were normalized to the signal from the protein of interest. If two or more gels were used for detecting different proteins from a single set of samples, all gels were run and transferred to the PVDF membranes together in a single buffer system and the Western blotting was conducted simultaneously for all membranes.

F-actin to G-actin ratio

The ratio of filamentous actin (F-actin) to globular actin (G-actin) ratio was evaluated as previously described (Huang *et al*, 2013; Pyronneau *et al*, 2017). Cortical brains or cultured cortical neurons were isolated and homogenized in cold lysis buffer containing (in mM): 100 NaF, 50 KCl, 10 K_2HPO_4, 2 $MgCl_2$, 1 EGTA, 1 sucrose, 0.2 dithiothreitol, 0.5% Triton X-100 (pH 7.0), followed by centrifugation at 15,000 g for 30 min at 4°C. The supernatant was used for measurement of soluble actin (G-actin). The insoluble F-actin from the pellet was resuspended and incubated in lysis buffer with an equal volume of buffer containing (in mM): 20 Tris–HCl, 1.5 GuHCl, 1 NaOAc, 1 $CaCl_2$, 1 ATP (pH 7.5) on ice for 1 h to convert F-actin into soluble G-actin, with gentle mixing every 15 min. The samples were centrifuged at 15,000 g for 30 min at 4°C, and F-actin was measured in this supernatant. Samples from the supernatant (G-actin) and pellet (F-actin) fractions were proportionally loaded and analyzed by Western blotting using an anti-actin antibody.

Chemical LTP induction

Chemical LTP (cLTP) was induced following a previously published study (Hussain *et al*, 2014). Briefly, cultured neurons were maintained 20 min in normal artificial cerebrospinal fluid (aCSF, 125 mM NaCl, 25 mM HEPES, 2.5 mM KCl, 1.5 mM $CaCl_2$, 1 mM MgCl, 33 mM Glucose, 0.5 μM TTX, 20 μM Bicuculline, 1 μM Strychnine; pH 7.4) before 10-min cLTP induction in magnesium-free aCSF supplemented with 200 μM glycine. After the cLTP induction, neurons were recovered in normal aCSF for 10 or 30 min before subjecting to Western blotting or immunocytochemistry experiments.

mEPSC recording

Whole-cell patch-clamp recordings were performed at room temperature (23-25°C) in a submersion chamber continuously perfused with aCSF containing (in mM): 119 NaCl, 2.5 KCl, 4 $CaCl_2$, 4 $MgCl_2$, 1 NaH_2PO_4, 26 $NaHCO_3$ and 11 D-Glucose, saturated with 95% O_2/5% CO_2 (pH 7.4, 310 mOsm). aCSF was supplemented with 1 μM TTX and 100 μM picrotoxin for miniature excitatory postsynaptic current (mEPSC) measurements to block action potential-dependent EPSCs and $GABA_A$ receptors, respectively. Whole-cell recording pipettes (~4–6 MΩ) were filled with intracellular solution containing (in mM): 130 K-gluconate, 6 KCl, 3 NaCl, 10 HEPES, 0.2 EGTA, 4 Mg-ATP, 0.4 Na-GTP, 14 Tris-phosphocreatine, 2 QX-314 (pH 7.25, 285 mOsm). Neurons at DIV 14–17 were used for electrophysiological analyses. Membrane potential was clamped at −60 mV. Neurons were not included in analyses if the resting membrane potential was > −45 mV, access resistance was >25 MΩ, or access resistance changed by > 20%. All recordings were performed with Clampex 10.6 and Multiclamp 700B amplifier interfaced with Digidata 1550B data acquisition system (Molecular Devices). Recordings were filtered at 1 kHz and digitized at 10 kHz. mEPSCs were analyzed with Mini Analysis Program (Synaptosoft) with a 5-pA threshold level.

Acute hippocampal slice preparation and fEPSP recording

Acute hippocampal slices were prepared from 6- to 8-week-old Nedd4-2 WT and Nedd4-2 cKO mice. Mice were anesthetized with

isoflurane inhalation, and the brain was rapidly removed and placed in ice-cold sucrose-based cutting solution containing the following (in mM): 220 sucrose, 2.5 KCl, 1 Na_2HPO_4, 2.5 $MgCl_2$, 0.5 $CaCl_2$, 26 $NaHCO_3$, and 20 D-glucose, saturated with 95% O_2/5% CO_2 (pH 7.4, 305 mOsm). Transverse hippocampal slices (400 μm) were cut using a McIlwain Tissue chopper (Ted Pella). Slices were transferred to a holding chamber in aCSF containing the following (in mM): 124 NaCl, 2.5 KCl, 2.5 $CaCl_2$, 1.3 $MgSO_4$, 1.25 NaH_2PO_4, 26 $NaHCO_3$, and 10 D-glucose (pH 7.4, 295-305 mOsm) for recovery for 30 min at 37°C and subsequently maintained at room temperature (23-25°C) for at least 60 min until use under oxygenation with 95% O_2/5% CO_2. For experiments involving the use of TAT or TAT-pS3 peptides, slices were preincubated with TAT or TAT-pS3 (20 μM) for 60 min before recording. After recovery incubation, extracellular field excitatory postsynaptic potential (fEPSP) recordings were carried out at 32°C (TC-324B; Warner Instrument). The slices were placed in a submerged chamber perfused with aCSF at the rate of 2 ml/min. A concentric bipolar stimulating electrode (CBARC75; FHC) was placed in the Schaffer collaterals of CA3, and extracellular fEPSPs were recorded using a glass capillary (TW150F-4; World Precision Instruments). Recording pipettes had resistances of 2–3 MΩ filled with aCSF, placed in the CA1 stratum radiatum. Test stimuli were given at every 20 s, and stimulus intensity adjusted to evoke approximately 40% of maximal response. A stable baseline was recorded for at least 20–30 min before inducing long-term potentiation (LTP). Early-phase LTP (E-LTP) was produced with a single train of high-frequency stimulation (HFS, 100 Hz stimulus for 1 s). Late-phase LTP (L-LTP) was produced with four HFS (100 Hz stimulus for 1 s) presented at 5-min intervals. fEPSP slope was measured by 20-80% of maximum negative deflection. fEPSPs were recorded using a Multiclamp 700B amplifier and digitized with a Digidata 1550B (Molecular Devices). Data were analyzed using pClamp software (version 10.6; Molecular Devices).

Behavioral testing

Mice, both male and female, were allowed to habituate to the testing room for at least 30 min before each test. The background sound was kept around 65 dB, and the tests were performed during the light phase in a dimly lit room (<50 lux) with indirect lighting on the testing area to minimize fear and anxiety-like behavior (Bouwknecht *et al*, 2007; Kastenberger *et al*, 2012; Puschban *et al*, 2016). All behavioral equipment was cleaned with 70% ethanol before and after each use.

Open field test

The open field test was performed as described (Zombeck *et al*, 2011). Mice were placed in the center of an open field arena (67 cm × 67 cm × 31 cm) and allowed for exploring for 5 min. Average velocity, distance traveled, immobile time, number of entries in the central zone, and duration in the central zone (35 cm × 35 cm) were measured continuously following overhead video tracking. The moving trajectory was visualized and analyzed using AnimalTracker software (Gulyas *et al*, 2016).

Novel object recognition test

Novel object recognition test was as described (Ujjainwala *et al*, 2019), which lasted a total of 3 days. On day 0 (habituation trial), mice were habituated to the testing chamber (25 cm × 25 cm) for 10 min without any added objects for habituation. On day 1 (training trial), mice were placed in the testing chamber and allowed to freely explore the chamber for 10 min with two identical objects (plastic block toys). On day 2 (testing trial), the chamber was set up with one familiar object and one novel object. The mice were placed in the testing chamber and allowed to freely explore for 10 min before being returned to the home cage. To determine phobic response to the objects, a different cohort of mice were presented with both projects as novel at the same time and allowed to explore for 10 min. Interaction with an object was defined as nose sniffing and head orientation within < 1.0 cm of an object, without any further interaction with the object (e.g., biting or climbing). The preference index was calculated by time spent exploring the novel object (T_{nov}) and dividing by total exploration time [preference index = $T_{nov}/(T_{nov} + T_{fam}) \times 100$] (Lueptow, 2017).

Barnes maze test

Barnes maze test was performed on a gray circular platform (91.44 cm diameter) with 20 evenly spaced holes around the perimeter to examine hippocampus-dependent spatial learning and memory as described (Schoberleitner *et al*, 2019; Ujjainwala *et al*, 2019). The bright illumination (1200 lux) was used as negative reinforcement to promote the motivation of mice to find the escape hole. The test consists of 4 separate phases, adaptation session (day 0), spatial acquisition sessions (days 1–4), short-term probe trial session (day 5), and long-term probe trial session (day 12). On day 0, each mouse was placed onto a platform for 5 min to explore the maze with the target hole. During acquisition trials at days 1-4, the mouse was placed in the maze for a maximum of 5 min. If the mouse found the target hole, the escape box was closed, and the mouse was kept in the box for 2 min to allow for the mouse to associate the escape box as a secure place. If the mouse did not find the target hole during the allotted time, it was then gently guided to the hole. Three trials a day were conducted with 20- to 30-min intertrial intervals when mice were returned to the home cage. For evaluation of acquisition sessions, the escape latency and the number of errors were determined. Errors were defined as nose pokes and head deflections over any hole that did not have the escape box beneath it. On day 5 (assessment of short-term memory) and on day 12 (long-term memory), respectively, escape box under the target hole was removed and the mouse was free to explore the maze for 2 min. Between the two test sessions, mice were kept in their home cages. For assessment of probe trial sessions, the circular platform was divided into quadrants, and time spent in target and opposite quadrants was measured.

Contextual fear conditioning test

Contextual fear conditioning test was performed as previously described (Clark *et al*, 2008), which lasted a total of 2 days. On day1 (training session), mice were individually placed in a fear conditioning chamber (32 cm × 28 cm × 30 cm) for 180 s with a metal grid floor that delivers shock stimuli under the control of a digital timer (Med Associates, St. Albans, VT). During the training phase, mice in the "fear" group received 2 footshocks (0.5 mA, 2 s duration) at 120 and 150 s. The response to the stimuli,

demonstrated by the velocity, distance traveled, and duration of freezing, was quantified after the second shock during the training day. Mice in the control group did not receive any footshocks. On day 2 (testing session), mice were placed in the chamber for 180 s without any footshocks. Trails were recorded, and the total percentage of time spent freezing was measured.

Experimental design and statistical analysis

For preparing neuronal cultures, both male and female mice were used. At least 3 l, randomized 4–6 mice each, were used in each experiment. For behavioral assays, both male and female mice at 6–8 weeks of age were used. Because *Nedd4-2*-dependent learning and memory behavior was only observed in male mice, only male mice at 6–8 weeks of age were used to prepare hippocampal slices for LTP experiments. Due to the design of our research, no blinding was performed. The data presented in this study have been tested for normality using the Kolmogorov–Smirnov test. The sample size was estimated by G*Power 3.1. Student's *t*-test was used when two conditions or groups were compared. One-way ANOVA with *post hoc* Tukey HSD (honestly significant difference) test was used for multiple comparison. Sample numbers, including the numbers of cells, slices, or repeats, are indicated in the figure legends. Differences are considered significant at the level of $p < 0.05$. Data analyses were performed using OriginPro 2019 (OriginLab).

Data availability

This study includes no data deposited in external repositories.

Expanded View for this article is available online.

Acknowledgements
This work is supported by the startup fund provided by the School of Molecular and Cellular Biology, University of Illinois at Urbana-Champaign, by National Institute of Health (R01NS105615 to N-P.T.), and by Brain and Behavioral Research Foundation NARSAD Young Investigator Grant (27018 to N-P.T.).

Author contributions
KYL and N-PT designed the research. KYL, JZ, and CAC performed the research and analyzed the data. CAC-H and JSR provided critical experimental resources and conceptual advance in developing the project. KYL and N-PT wrote the manuscript. All authors read and approved the final manuscript.

Conflict of interest
The authors declare that they have no conflict of interest.

References

Allen AS, Berkovic SF, Cossette P, Delanty N, Dlugos D, Eichler EE, Epstein MP, Glauser T, Goldstein DB, Han Y *et al* (2013) De novo mutations in epileptic encephalopathies. *Nature* 501: 217 – 221

Ambach A, Saunus J, Konstandin M, Wesselborg S, Meuer SC, Samstag Y (2000) The serine phosphatases PP1 and PP2A associate with and activate the actin-binding protein cofilin in human T lymphocytes. *Eur J Immunol* 30: 3422 – 3431

Asinof S, Mahaffey C, Beyer B, Frankel WN, Boumil R (2016) Dynamin 1 isoform roles in a mouse model of severe childhood epileptic encephalopathy. *Neurobiol Dis* 95: 1 – 11

Baharani A, Wei Z, Roesler WJ, Mousseau DD (2020) A Progressive loss of phosphoSer138-profilin aligns with symptomatic course in the R6/2 mouse model of huntington's disease: possible sex-dependent signaling. *Cell Mol Neurobiol* https://doi.org/10.1007/s10571-020-00984-2

Bamburg JR (1999) Proteins of the ADF/cofilin family: essential regulators of actin dynamics. *Annu Rev Cell Dev Biol* 15: 185 – 230

Bamburg JR, Bernstein BW (2010) Roles of ADF/cofilin in actin polymerization and beyond. *F1000 Biol Rep* 2: 62

Bednarek N, Motte J, Soufflet C, Plouin P, Dulac O (1998) Evidence of late-onset infantile spasms. *Epilepsia* 39: 55 – 60

Boase NA, Rychkov GY, Townley SL, Dinudom A, Candi E, Voss AK, Tsoutsman T, Semsarian C, Melino G, Koentgen F *et al* (2011) Respiratory distress and perinatal lethality in Nedd4-2-deficient mice. *Nat Commun* 2: 287

Bouwknecht JA, Spiga F, Staub DR, Hale MW, Shekhar A, Lowry CA (2007) Differential effects of exposure to low-light or high-light open-field on anxiety-related behaviors: relationship to c-Fos expression in serotonergic and non-serotonergic neurons in the dorsal raphe nucleus. *Brain Res Bull* 72: 32 – 43

Broix L, Jagline H, L Ivanova E, Schmucker S, Drouot N, Clayton-Smith J, Pagnamenta AT, Metcalfe KA, Isidor B, Louvier UW *et al* (2016) Mutations in the HECT domain of NEDD4L lead to AKT-mTOR pathway deregulation and cause periventricular nodular heterotopia. *Nat Genet* 48: 1349 – 1358

Chen J, Huang C, Chen K, Li S, Zhang X, Cheng J, Cai M, Xiao Y (2018) Overexpression of LBH is associated with poor prognosis in human hepatocellular carcinoma. *Onco Targets Ther* 11: 441 – 448

Cingolani LA, Goda Y (2008) Actin in action: the interplay between the actin cytoskeleton and synaptic efficacy. *Nat Rev Neurosci* 9: 344 – 356

Clark PJ, Brzezinska WJ, Thomas MW, Ryzhenko NA, Toshkov SA, Rhodes JS (2008) Intact neurogenesis is required for benefits of exercise on spatial memory but not motor performance or contextual fear conditioning in C57BL/6J mice. *Neuroscience* 155: 1048 – 1058

Dibbens LM, Ekberg J, Taylor I, Hodgson BL, Conroy SJ, Lensink IL, Kumar S, Zielinski MA, Harkin LA, Sutherland GR *et al* (2007) NEDD4-2 as a potential candidate susceptibility gene for epileptic photosensitivity. *Genes Brain Behav* 6: 750 – 755

Dillon C, Goda Y (2005) The actin cytoskeleton: integrating form and function at the synapse. *Annu Rev Neurosci* 28: 25 – 55

Duffney LJ, Wei J, Cheng J, Liu W, Smith KR, Kittler JT, Yan Z (2013) Shank3 deficiency induces NMDA receptor hypofunction via an actin-dependent mechanism. *J Neurosci* 33: 15767 – 15778

Ekberg J, Schuetz F, Boase NA, Conroy SJ, Manning J, Kumar S, Poronnik P, Adams DJ (2007) Regulation of the voltage-gated K(+) channels KCNQ2/3 and KCNQ3/5 by ubiquitination. Novel role for Nedd4-2. *J Biol Chem* 282: 12135 – 12142

Epstein PM, Curti M, Jansson I, Huang CK, Schenkman JB (1989) Phosphorylation of cytochrome P450: regulation by cytochrome b5. *Arch Biochem Biophys* 271: 424 – 432

Fukazawa Y, Saitoh Y, Ozawa F, Ohta Y, Mizuno K, Inokuchi K (2003) Hippocampal LTP is accompanied by enhanced F-actin content within the dendritic spine that is essential for late LTP maintenance in vivo. *Neuron* 38: 447 – 460

Goel P, Manning JA, Kumar S (2015) NEDD4-2 (NEDD4L): the ubiquitin ligase for multiple membrane proteins. *Gene* 557: 1 – 10

Gorski JA, Talley T, Qiu M, Puelles L, Rubenstein JL, Jones KR (2002) Cortical excitatory neurons and glia, but not GABAergic neurons, are produced in the Emx1-expressing lineage. *J Neurosci* 22: 6309 – 6314

Gulyas M, Bencsik N, Pusztai S, Liliom H, Schlett K (2016) AnimalTracker: an ImageJ-Based tracking API to create a customized behaviour analyser program. *Neuroinformatics* 14: 479 – 481

Hsia H-e, Kumar R, Luca R, Takeda M, Courchet J, Nakashima J, Wu S, Goebbels S, An W, Eickholt Bj *et al* (2014) Ubiquitin E3 ligase Nedd4-1 acts as a downstream target of PI3K/PTEN-mTORC1 signaling to promote neurite growth. *Proc Natl Acad Sci USA* 111: 13205 – 13210

Hu M, Huang H, Zhao R, Li P, Li M, Miao H, Chen N, Chen M (2014) AZD8055 induces cell death associated with autophagy and activation of AMPK in hepatocellular carcinoma. *Oncol Rep* 31: 649 – 656

Huang W, Zhu PJ, Zhang S, Zhou H, Stoica L, Galiano M, Krnjevic K, Roman G, Costa-Mattioli M (2013) mTORC2 controls actin polymerization required for consolidation of long-term memory. *Nat Neurosci* 16: 441 – 448

Hussain NK, Diering GH, Sole J, Anggono V, Huganir RL (2014) Sorting Nexin 27 regulates basal and activity-dependent trafficking of AMPARs. *Proc Natl Acad Sci USA* 111: 11840 – 11845

Jewett KA, Zhu J, Tsai NP (2015) The tumor suppressor p53 guides GluA1 homeostasis through Nedd4-2 during chronic elevation of neuronal activity. *J Neurochem* 135: 226 – 233

Kastenberger I, Lutsch C, Herzog H, Schwarzer C (2012) Influence of sex and genetic background on anxiety-related and stress-induced behaviour of prodynorphin-deficient mice. *PLoS One* 7: e34251

Kato K, Miya F, Hori I, Ieda D, Ohashi K, Negishi Y, Hattori A, Okamoto N, Kato M, Tsunoda T *et al* (2017) A novel missense mutation in the HECT domain of NEDD4L identified in a girl with periventricular nodular heterotopia, polymicrogyria and cleft palate. *J Hum Genet* 62: 861 – 863

Kim JE, Lee DS, Kim MJ, Kang TC (2019) PLPP/CIN-mediated NEDD4-2 S448 dephosphorylation regulates neuronal excitability via GluA1 ubiquitination. *J Neurochem* 10: 545

Kim T, Chokkalla AK, Vemuganti R (2021) Deletion of ubiquitin ligase Nedd4l exacerbates ischemic brain damage. *J Cereb Blood Flow Metab* 41: 1058 – 1066

Laedermann CJ, Cachemaille M, Kirschmann G, Pertin M, Gosselin R-D, Chang I, Albesa M, Towne C, Schneider BL, Kellenberger S *et al* (2013) Dysregulation of voltage-gated sodium channels by ubiquitin ligase NEDD4-2 in neuropathic pain. *J Clin Investig* 123: 3002 – 3013

Lee KY, Jewett KA, Chung HJ, Tsai NP (2018) Loss of fragile X protein FMRP impairs homeostatic synaptic downscaling through tumor suppressor p53 and ubiquitin E3 ligase Nedd4-2. *Hum Mol Genet* 27: 2805 – 2816

Li Y, Hu F, Chen HJ, Du YJ, Xie ZY, Zhang Y, Wang J, Wang Y (2014) LIMK-dependent actin polymerization in primary sensory neurons promotes the development of inflammatory heat hyperalgesia in rats. *Sci Signal* 7: ra61

Lin B, Kramár EA, Bi X, Brucher FA, Gall CM, Lynch G (2005) Theta stimulation polymerizes actin in dendritic spines of hippocampus. *J Neurosci* 25: 2062 – 2069

Liu DC, Eagleman DE, Tsai NP (2019) Novel roles of ER stress in repressing neural activity and seizures through Mdm2- and p53-dependent protein translation. *PLoS Genet* 15: e1008364

Lu W, Man H, Ju W, Trimble WS, MacDonald JF, Wang YT (2001) Activation of synaptic NMDA receptors induces membrane insertion of new AMPA receptors and LTP in cultured hippocampal neurons. *Neuron* 29: 243 – 254

Lueptow LM (2017) Novel object recognition test for the investigation of learning and memory in mice. *J Vis Exp* 126: 55718

Luo L (2002) Actin cytoskeleton regulation in neuronal morphogenesis and structural plasticity. *Annu Rev Cell Dev Biol* 18: 601 – 635

Mizuno K (2013) Signaling mechanisms and functional roles of cofilin phosphorylation and dephosphorylation. *Cell Signal* 25: 457 – 469

Moriyama K, Iida K, Yahara I (1996) Phosphorylation of Ser-3 of cofilin regulates its essential function on actin. *Genes Cells* 1: 73 – 86

Nicoll RA (2017) A brief history of long-term potentiation. *Neuron* 93: 281 – 290

Niere F, Wilkerson JR, Huber KM (2012) Evidence for a fragile X mental retardation protein-mediated translational switch in metabotropic glutamate receptor-triggered Arc translation and long-term depression. *J Neurosci* 32: 5924 – 5936

Ohashi K (2015) Roles of cofilin in development and its mechanisms of regulation. *Dev Growth Differ* 57: 275 – 290

Oleinik NV, Krupenko NI, Krupenko SA (2010) ALDH1L1 inhibits cell motility via dephosphorylation of cofilin by PP1 and PP2A. *Oncogene* 29: 6233 – 6244

Pavone P, Polizzi A, Marino SD, Corsello G, Falsaperla R, Marino S, Ruggieri M (2020) West syndrome: a comprehensive review. *Neurol Sci* 41: 3547 – 3562

Pfeiffer BE, Huber KM (2007) Fragile X mental retardation protein induces synapse loss through acute postsynaptic translational regulation. *J Neurosci* 27: 3120 – 3130

Price MG, Yoo JW, Burgess DL, Deng F, Hrachovy RA, Frost Jr JD, Noebels JL (2009) A triplet repeat expansion genetic mouse model of infantile spasms syndrome, Arx(GCG)10+7, with interneuronopathy, spasms in infancy, persistent seizures, and adult cognitive and behavioral impairment. *J Neurosci* 29: 8752 – 8763

Puschban Z, Sah A, Grutsch I, Singewald N, Dechant G (2016) Reduced anxiety-like behavior and altered hippocampal morphology in female p75NTR(exon IV-/-) mice. *Front Behav Neurosci* 10: 103

Pyronneau A, He Q, Hwang JY, Porch M, Contractor A, Zukin RS (2017) Aberrant Rac1-cofilin signaling mediates defects in dendritic spines, synaptic function, and sensory perception in fragile X syndrome. *Sci Signal* 10: eaan0852

Rust MB, Gurniak CB, Renner M, Vara H, Morando L, Görlich A, Sassoè-Pognetto M, Banchaabouchi MA, Giustetto M, Triller A *et al* (2010) Learning, AMPA receptor mobility and synaptic plasticity depend on n-cofilin-mediated actin dynamics. *EMBO J* 29: 1889 – 1902

Salar S, Moshé SL, Galanopoulou AS (2018) Metabolic etiologies in West syndrome. *Epilepsia Open* 3: 134 – 166

Schoberleitner I, Mutti A, Sah A, Wille A, Gimeno-Valiente F, Piatti P, Kharitonova M, Torres L, López-Rodas G, Liu JJ *et al* (2019) Role for chromatin remodeling factor Chd1 in learning and memory. *Front Mol Neurosci* 12: 3

Schuetz F, Kumar S, Poronnik P, Adams DJ (2008) Regulation of the voltage-gated K(+) channels KCNQ2/3 and KCNQ3/5 by serum- and glucocorticoid-regulated kinase-1. *Am J Physiol Cell Physiol* 295: C73 – C80

Sudhof TC, Malenka RC (2008) Understanding synapses: past, present, and future. *Neuron* 60: 469 – 476

Takeuchi T, Duszkiewicz AJ, Morris RG (2014) The synaptic plasticity and memory hypothesis: encoding, storage and persistence. *Philos Trans R Soc Lond B Biol Sci* 369: 20130288

Toshima J, Toshima JY, Amano T, Yang N, Narumiya S, Mizuno K (2001) Cofilin phosphorylation by protein kinase testicular protein kinase 1 and its role in integrin-mediated actin reorganization and focal adhesion formation. *Mol Biol Cell* 12: 1131 – 1145

Tsai NP, Wilkerson JR, Guo W, Maksimova MA, DeMartino GN, Cowan CW, Huber KM (2012) Multiple autism-linked genes mediate synapse elimination via proteasomal degradation of a synaptic scaffold PSD-95. *Cell* 151: 1581 – 1594

Ujjainwala AL, Courtney CD, Wojnowski NM, Rhodes JS, Christian CA (2019) Differential impacts on multiple forms of spatial and contextual memory in diazepam binding inhibitor knockout mice. *J Neurosci Res* 97: 683 – 697

Wang Y, Dong Q, Xu XF, Feng X, Xin J, Wang DD, Yu H, Tian T, Chen ZY (2013) Phosphorylation of cofilin regulates extinction of conditioned aversive memory via AMPAR trafficking. *J Neurosci* 33: 6423 – 6433

Wu Y, Luo X, Liu X, Liu D, Wang X, Guo Z, Zhu L, Tian Q, Yang X, Wang JZ (2015) Intraperitoneal administration of a novel TAT-BDNF peptide ameliorates cognitive impairments via modulating multiple pathways in two Alzheimer's rodent models. *Sci Rep* 5: 15032

Yanpallewar S, Wang T, Koh DC, Quarta E, Fulgenzi G, Tessarollo L (2016) Nedd4-2 haploinsufficiency causes hyperactivity and increased sensitivity to inflammatory stimuli. *Sci Rep* 6: 32957

Yuen EY, Yan Z (2009) Dopamine D4 receptors regulate AMPA receptor trafficking and glutamatergic transmission in GABAergic interneurons of prefrontal cortex. *J Neurosci* 29: 550 – 562

Yuskaitis CJ, Ruzhnikov MRZ, Howell KB, Allen IE, Kapur K, Dlugos DJ, Scheffer IE, Poduri A, Sherr EH (2018) Infantile spasms of unknown cause: predictors of outcome and genotype-phenotype correlation. *Pediatr Neurol* 87: 48 – 56

Zhu J, Lee KY, Jewett KA, Man HY, Chung HJ, Tsai NP (2017) Epilepsy-associated gene Nedd4-2 mediates neuronal activity and seizure susceptibility through AMPA receptors. *PLoS Genet* 13: e1006634

Zhu J, Lee KY, Jong TT, Tsai NP (2019) C2-lacking isoform of Nedd4-2 regulates excitatory synaptic strength through GluA1 ubiquitination-independent mechanisms. *J Neurochem* 151: 289 – 300

Zombeck JA, Deyoung EK, Brzezinska WJ, Rhodes JS (2011) Selective breeding for increased home cage physical activity in collaborative cross and Hsd: ICR mice. *Behav Genet* 41: 571 – 582

